GEOPHYSICS, VOL. 55, NO. 4 (APRIL 1990); P. 410–421, 11 FIGS.

DOI:10.1190/1.1442850

Split-step Fourier migration

P. L. Stoffa*, J. T. Fokkema‡, R. M. de Luna Freire§, and W. P. Kessinger*

ABSTRACT

The split-step Fourier method is developed and applied to migrating stacked seismic data in two and three dimensions. This migration method, which is implemented in both the frequency-wavenumber and frequency-space domains, takes into account laterally varying velocity by defining a reference slowness (reciprocal of velocity) as the mean slowness in the migration interval and a perturbation term that is spatially varying. The mean slowness defines a reference vertical wavenumber which is used in the frequency-wavenumber domain to downward continue the data across a depth interval as in constant-velocity phase-shift migration. The perturbation term is used to define a "source" contribution that is taken into account by the application of a second phase shift in the frequency-space domain. Since the method does not include the effects of second and higher order spatial derivatives of the slowness field, the method theoretically is accurate only when there are no rapid lateral slowness variations combined with steep angles of propagation. However, synthetic and real examples indicate that good results are obtained for realistic geologic structures.

INTRODUCTION

Migration methods differ primarily by their method of implementation. Finite-difference approximations to the wave equation accommodate lateral velocity variations, but the differential operators required by the wave equation must be approximated (Baysal et al., 1983). Depending on the order of the approximation used, the spatial sampling, and whether the implementation is implicit or explicit, problems in accuracy and stability may arise. In phase-shift migration, which is implemented in the frequency-wavenumber domain (Stolt, 1978; Gazdag, 1978), the differential operators are applied exactly and the method is unconditionally stable. However, because the wave equation is solved in the frequency-wavenumber domain, a constant velocity must be used for each depth interval being migrated. Gazdag and Sguazzero (1984) introduced phase shift plus interpolation as one way to circumvent this problem. In this case, several constant-velocity migrations are performed for each migration interval and the results are combined to form the final migrated image. In this approach, each constant-velocity migration requires the application of a phase shift, followed by an inverse spatial Fourier transform. Pai (1985, 1988) generalized frequency-wavenumber migration to accommodate arbitrary velocity variations. Pai's method is based on a matrix integral formulation that takes into account the coupling between plane-wave components due to lateral velocity variations. Kosloff and Kessler (1987) developed a similar formulation but used a Chebychev series expansion to the formal solution for the downward continued pressure wave field and its vertical derivative.

The split-step Fourier method is an alternative to the above methods. It is based on a modification to phase-shift migration that makes it possible to accommodate lateral changes in the velocity for each migration interval. The method was first employed by Hardin and Tappert (1973), Tappert (1974), and then by McDaniel (1975) to model horizontal sound transmission in a stratified water column overlying sediment. The original development was based on the parabolic approximation to the acoustic wave equation. Here the method is developed using the exact vertical wavenumber as demonstrated by Freire (1988). If a migration interval has no lateral velocity variation, the method is exact and the wavenumber is correct up to 90 degrees. Also, if the propagation is vertical, the method is exact for any lateral velocity variation.

The split-step Fourier method is of interest because it has the advantages of phase-shift migration but can still accom-

Presented at the 56th Annual International Meeting, Society of Exploration Geophysicists. Manuscript received by the Editor February 27, 1989; revised manuscript received October 6, 1989.
*Department of Geological Sciences, Institute for Geophysics, University of Texas at Austin, 8701 Mopac Boulevard, Austin, Texas 78759-8345.
‡Formerly PPPG/UFBa, Salvador, Bahia, Brasil; presently Delft University of Technology, P.O. Box 5028, 2600 GA Delft, The Netherlands.
§Formerly PPPG/UFBa, Salvador, Bahia, Brasil; presently Petrobras/Dexba /Dirgef, Av. Beira Mar 220, Salvador, Bahia, Brasil 40010.

modate lateral velocity variations. The lateral velocity variations are taken into account as a perturbation, and consequently only one additional spatial Fourier transform is required for each depth extrapolation. This behavior contrasts with phase shift plus interpolation, which requires a complete phase-shift migration, including the Fourier transform, for each velocity used in the depth extrapolation. By taking into account lateral velocity variations (without the need for multiple phase-shift migrations), the split-step Fourier method makes it practical to realize the advantages of phase-shift migration. Some of these advantages are faithful migration of the frequency band of interest, accurate implementation of the differential operators, unconditional stability, and the ability to migrate through a large layer in one step, e.g., the water column in offshore areas. Computationally, the split-step Fourier method also has the advantage that only the frequencies of interest must be migrated, a result particularly valuable in three-dimensional (3-D) migration, because it may be possible to solve the problem in computer memory without the need for costly transfers to and from disk.

OVERVIEW OF THE SPLIT-STEP FOURIER MIGRATION METHOD

In a recent paper by Wen et al. (1988), 3-D modeling and migration were discussed using a Fourier transform approach. In Wen's paper, as in most previous papers that employ Fourier transform methods to solve the acoustic wave equation, a constant lateral velocity is required. In the split-step Fourier method, the interval slowness (reciprocal of interval velocity) is divided into two terms: a constant reference slowness and a perturbation term. The reference slowness is used to migrate across the interval in the frequency-wavenumber domain just as in the case of constant-velocity phase-shift migration, but the inclusion of the perturbation term results in a correction which is applied in the frequency-space domain as a second phase shift.

Consider the propagation of compressional waves in an acoustic constant-density medium using the wave equation:

$$\nabla^2 p - u^2 \frac{\partial^2}{\partial t^2} p = 0, \tag{1}$$

where $p = p(x, y, z, t)$ is the pressure and $u = u(x, y, z)$ is the medium slowness, which is defined as the inverse of half the propagation velocity $u(x, y, z) = 2/v(x, y, z)$ as required by the exploding reflector model (Loewenthal et al., 1976).

After transforming equation (1) into the frequency domain, we have

$$\nabla^2 P + \omega^2 u^2 P = 0, \tag{2}$$

where

$$P(\mathbf{r}, z, \omega) = \int_{-\infty}^{\infty} p(\mathbf{r}, z, t)\, e^{-i\omega t}\, dt, \tag{3}$$

and $\mathbf{r}$ is the horizontal position vector defined through $\mathbf{r} = x\mathbf{i}_x + y\mathbf{i}_y$ with

$$r = |\mathbf{r}| = \sqrt{x^2 + y^2}.$$

We decompose the slowness field $u(\mathbf{r}, z)$ into two components:

$$u(\mathbf{r}, z) = u_0(z) + \Delta u(\mathbf{r}, z), \tag{4}$$

where we define $u_0(z)$ as the reference slowness which we will specify as the mean. All variations are accommodated by the $\Delta u(\mathbf{r}, z)$ component. Substituting into equation (2), we have

$$\nabla^2 P + \omega^2 u_0^2 P = -\omega^2 (2 u_0 \Delta u + \Delta u^2) P, \tag{5}$$

or

$$\nabla^2 P + \omega^2 u_0^2 P = -S(\mathbf{r}, z, \omega), \tag{6}$$

where S is defined as

$$S(\mathbf{r}, z, \omega) = \omega^2 [2 u_0 \Delta u(\mathbf{r}, z) + \Delta u^2(\mathbf{r}, z)] P(\mathbf{r}, z, \omega). \tag{7}$$

Thus, the homogeneous acoustic wave equation (2) has been transformed into the inhomogeneous wave equation (6) by the inclusion of a source-like term $S(\mathbf{r}, z, \omega)$ due to the slowness variations.

The solution to equation (6) that is used by the split-step Fourier method is based on ignoring the Δu^2 contribution and can be summarized as follows: Fourier transform the previously migrated upgoing wave field at depth z_n, $P_-(\mathbf{r}, z_n, \omega)$, from $\mathbf{r}$ to $\mathbf{k}_r$ space:

$$\tilde{P}_-(\mathbf{k}_r, z_n, \omega) = \int_{-\infty}^{\infty} \mathrm{P}_-(\mathbf{r}, z_n, \omega)\, e^{i\mathbf{k}_r \cdot \mathbf{r}}\, d\mathbf{r}, \tag{8}$$

where $\mathbf{k}_r$ is the horizontal wave vector defined by $\mathbf{k}_r = k_x \mathbf{i}_{k_x} + k_y \mathbf{i}_{k_y}$,

$$k_r = |\mathbf{k}_r| = \sqrt{k_x^2 + k_y^2}.$$

Apply a phase shift based on the vertical wavenumber computed using the reference slowness for all frequencies and wavenumbers:

$$\tilde{P}_1(\mathbf{k}_r, z_n, \Delta z, \omega) = \tilde{P}_-(\mathbf{k}_r, z_n, \omega)\, e^{ik_{z_0} \Delta z}, \tag{9}$$

where

$$k_{z_0} = \sqrt{\omega^2 u_0^2 - k_r^2} = \omega u_0 \sqrt{1 - (k_r/\omega u_0)^2} \tag{10}$$

and u_0 is the mean slowness for the interval Δz with Δz assumed to be small. Inverse Fourier transform the phase-shifted data $\tilde{P}_1(\mathbf{k}_r, z_n, \Delta z, \omega)$ from $\mathbf{k}_r$ to $\mathbf{r}$:

$$P_1(\mathbf{r}, z_n, \Delta z, \omega) = \left(\frac{1}{2\pi}\right)^2 \int_{-\infty}^{\infty} \tilde{P}_1(\mathbf{k}_r, z_n, \Delta z, \omega)\, e^{-i\mathbf{k}_r \cdot \mathbf{r}}\, d\mathbf{k}_r. \tag{11}$$

Next, apply a second phase shift due to the perturbation in the slowness, $\Delta u(\mathbf{r}, z) = u(\mathbf{r}, z) - u_0(z)$, in the interval Δz:

$$P_-(\mathbf{r}, z_{n+1}, \omega) = e^{i\omega \Delta u(\mathbf{r}, z) \Delta z} P_1(\mathbf{r}, z_n, \Delta z, \omega). \tag{12}$$

Integrate $P(\mathbf{r}, z_{n+1}, \omega)$ over all the frequencies of interest, e.g., ω_1 to ω_2, to obtain the migrated data for the current depth z_{n+1}:

$$p(\mathbf{r}, z_{n+1}, 0) = \left(\frac{1}{2\pi}\right)^2 \int_{\omega_1}^{\omega_2} P_-(\mathbf{r}, z_{n+1}, \omega)\, d\omega. \quad (13)$$

The first phase shift is identical to that employed for a constant-velocity phase-shift migration. The second phase shift acts as a correction term providing a time shift based on the difference between the actual and reference slownesses at each spatial position. Just as in other migration methods, this process is repeated for the next migration interval. For a 3-D problem, forward and inverse two-dimensional (2-D) complex-to-complex spatial Fourier transforms are required for each migration interval. This is the major computational requirement of the method. For a 2-D migration, only a one-dimensional (1-D) complex-to-complex spatial Fourier transform is required for each migration interval.

DERIVATION OF THE SPLIT-STEP FOURIER TRANSFORM MIGRATION METHOD

We now formally derive the method. The accuracy of the method is detailed in the Appendix. Equation (6), after a spatial Fourier transform, can be expressed in terms of the horizontal wave vector $\mathbf{k}_r$ as

$$\frac{\partial^2}{\partial z^2}\tilde{P} + (\omega^2 u_0^2 - k_r^2)\tilde{P} = -\tilde{S}, \quad (14)$$

where $\tilde{S}=\tilde{S}(\mathbf{k}_r, z, \omega)$.

We now rewrite equation (14) in terms of the reference vertical wavenumber k_{z_0}:

$$\frac{\partial^2}{\partial z^2}\tilde{P} + k_{z_0}^2\tilde{P} = -\tilde{S}, \quad (15)$$

where the reference vertical wavenumber k_{z_0} corresponds to the constant-slowness case described by equation (10), and where we choose the real part Re $\{k_{z_0}\} \geq 0$.

During migration, we extrapolate the upgoing wave field at depth z_n, $\tilde{P}_-(\mathbf{k}_r, z_n, \omega)$, downward to the next level z_{n+1}, ignoring any wave-field interactions. In poststack migration of common-midpoint (CMP) data, this is a reasonable approximation, since the effect of multiples can often be ignored. Including the effect of the source contribution, the required extrapolation is

$$\tilde{P}_-(\mathbf{k}_r, z_{n+1}, \omega) = \tilde{P}_-(\mathbf{k}_r, z_n, \omega)e^{ik_{z_0}\Delta z} - \int_{z_n}^{z_{n+1}} \frac{\exp\left[-ik_{z_0}(z' - z_{n+1})\right]}{2ik_{z_0}} \tilde{S}(\mathbf{k}_r, z', \omega)\, dz', \quad (16)$$

which is initiated by $\tilde{P}_-(\mathbf{k}_r, z_n, \omega) = \tilde{P}_-(\mathbf{k}_r, z_0, \omega)$, a known quantity. At this point, no restrictions have been made on the slowness field. Equation (16) could be solved numerically by integrating the source term for any arbitrary slowness variation.

To complete the development of the split-step Fourier method, we assume that the lateral variation of the slowness is small compared to the reference slowness u_0:

$$u_0 \gg |\Delta u(\mathbf{r}, z)|. \quad (17)$$

Consequently, source terms of the order Δu^2 can be dropped and, consistent with an assumption of no wave-field interaction, we replace the total wave field in equation (7) by the upgoing wave field. This leads to the following approximation of the source $S(\mathbf{r}, z, \omega)$:

$$S(\mathbf{r}, z, \omega) = 2\omega^2 u_0 \Delta u(\mathbf{r}, z) P_-(\mathbf{r}, z, \omega). \quad (18)$$

For migration, the reference slowness u_0 is specified for the depth interval z_n to z_{n+1}. That is, for each depth interval, we are free to redefine u_0 based on the true slowness field $u(\mathbf{r}, z)$ at this level. Since we expect the lateral slowness variation to be less than the vertical variation, this is a reasonable approximation.

Now, we consider the source term of equation (18) in more detail. The corresponding spatial Fourier transform is

$$\tilde{S}(\mathbf{k}_r, z, \omega) = 2\omega^2 u_0 \int_{-\infty}^{\infty} \Delta\tilde{u}(\mathbf{k}_r - \mathbf{k}_r', z)\tilde{P}_-(\mathbf{k}_r' z, \omega)\, d\mathbf{k}_r', \quad (19)$$

where $\Delta\tilde{u}(\mathbf{k}_r, z)$ is the spatial Fourier transform of $\Delta u(\mathbf{r}, z)$.

Substituting $\tilde{S}(\mathbf{k}_r, z, \omega)$ into the integral I of equation (16) and substituting for k_{z_0} from equation (10), we have

$$I = \int_{z_n}^{z_{n+1}} dz' \frac{\exp\{i\omega u_0[1 - (k_r/\omega u_0)^2]^{1/2}(z_{n+1} - z')\}}{2i\omega u_0[1 - (k_r/\omega u_0)^2]^{1/2}} \times 2\omega^2 u_0 \int_{-\infty}^{\infty} \Delta\tilde{u}(\mathbf{k}_r - \mathbf{k}_r', z')\, \tilde{P}_-(\mathbf{k}_r', z', \omega)\, d\mathbf{k}_r', \quad (20)$$

which, after expanding the denominator and keeping only the first term, simplifies to

$$I = -i\omega \int_{z_n}^{z_{n+1}} dz' \int_{-\infty}^{\infty} \Delta\tilde{u}(\mathbf{k}_r - \mathbf{k}_r', z') \times \tilde{P}_-(\mathbf{k}_r', z', \omega)\, e^{ik_{z_0}'(z_{n+1} - z')}\, d\mathbf{k}_r' + \varepsilon, \quad (21)$$

where

$$k_{z_0}' = \omega u_0[1 - (k_r'/\omega u_0)^2]^{1/2}, \quad (22)$$

and ε is the error term that is analyzed in the Appendix.

We now define $\tilde{P}_1(\mathbf{k}_r, z, d, \omega)$ as the upgoing wave field extrapolated to a depth between levels z_n and z_{n+1}. First, considering the slowness constant between z and $z + d$, we have

$$\tilde{P}_1(\mathbf{k}_r, z, d, \omega) = \tilde{P}_-(\mathbf{k}_r, z, \omega) \exp(ik_{z_0} d), \quad (23)$$

and consider

$$z_n \leq z \leq z_{n+1}$$

and

$$z_n \leq z + d \leq z_{n+1}, \quad (24)$$

where d is the nonnegative depth step of the extrapolation. In particular, we note

$$\tilde{P}_1(\mathbf{k}_r, z, 0, \omega) = \tilde{P}_-(\mathbf{k}_r, z, \omega). \quad (25)$$

Substituting equation (23) into equation (21) and neglecting the error term ε, we have

$$I = -i\omega \int_{z_n}^{z_{n+1}} dz' \int_{-\infty}^{\infty} \Delta\tilde{u}(\mathbf{k}_r - \mathbf{k}_r', z') \times \tilde{P}_1(\mathbf{k}_r', z', d_{n+1}, \omega)\, d\mathbf{k}_r', \quad (26)$$

where

$$d_{n+1}(z') = z_{n+1} - z'.$$

Substituting equation (26) into equation (16) results in

$$\tilde{P}_-(\mathbf{k}_r, z_{n+1}, \omega) = \tilde{P}_1(\mathbf{k}_r, z_n, \Delta z, \omega) + i\omega \int_{z_n}^{z_{n+1}} dz' \int_{-\infty}^{\infty} \Delta\tilde{u}(\mathbf{k}_r - \mathbf{k}_r', z')\, \tilde{P}_1(\mathbf{k}_r', z', d_{n+1}, \omega)\, d\mathbf{k}_r'. \quad (27)$$

Taking the inverse Fourier transform from $\mathbf{k}_r$ to $\mathbf{r}$ space, we can transform the convolution of $\Delta\tilde{u}$ with $\tilde{P}_1$ in the $\mathbf{k}_r$ domain to the product of their inverse Fourier transforms in the $\mathbf{r}$ domain:

$$P_-(\mathbf{r}, z_{n+1}, \omega) = P_1(\mathbf{r}, z_n, \Delta z, \omega) + i\omega \int_{z_n}^{z_{n+1}} dz' \Delta u(\mathbf{r}, z')\, P_1(\mathbf{r}, z', d_{n+1}, \omega), \quad (28)$$

where $P_1(\mathbf{r}, z, d, \omega)$ is defined as the inverse Fourier transform of $\tilde{P}_1(\mathbf{k}_r, z, d, \omega)$,

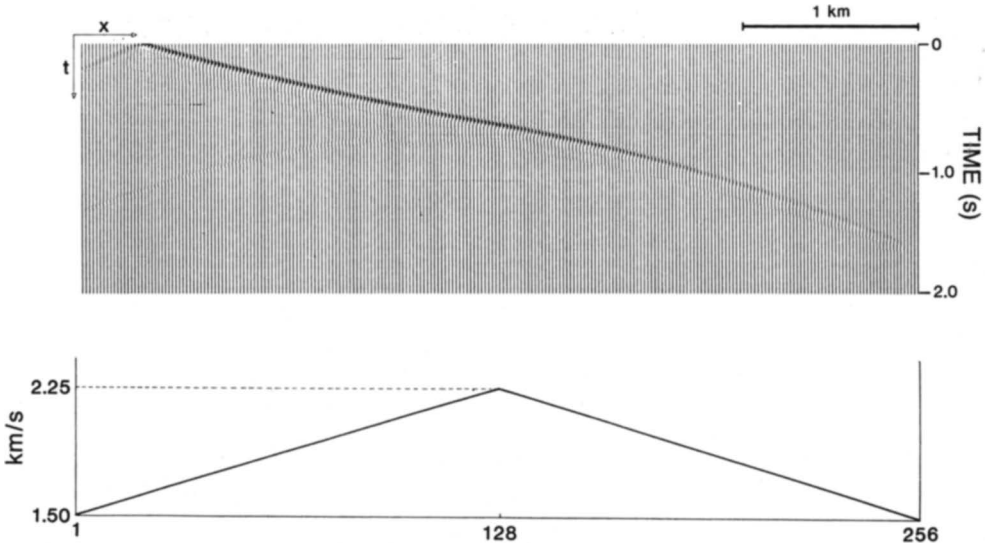

FIG. 1a. (upper) Synthetic seismic data for a 45° dipping reflection, where the velocity varies laterally as indicated (lower). In this example, Δx = 20 m and the sampling interval is 4 ms. 256 traces and 512 time samples were used.

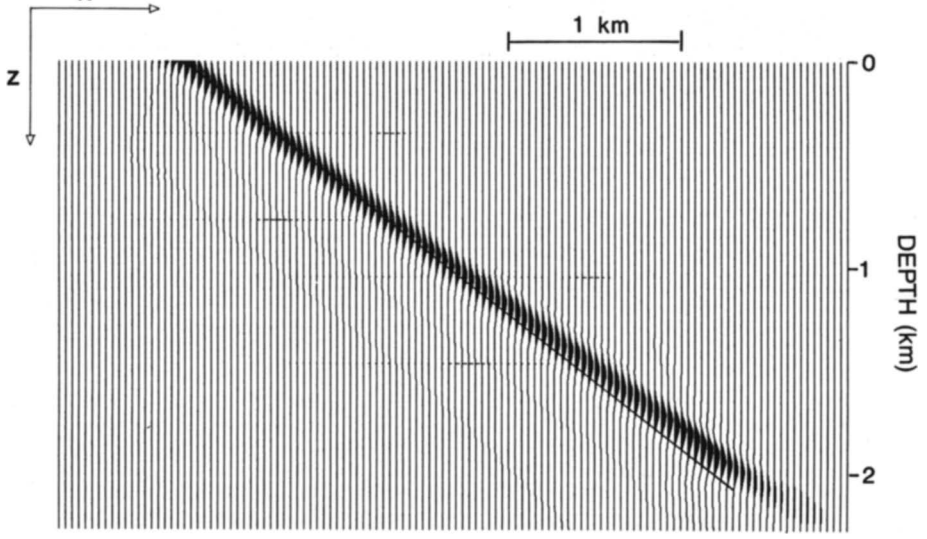

FIG. 1b. Migrated data of (a). The deviation of the migrated data from the proper position (as indicated by the solid line) is the greatest where the rays deviate significantly from vertical incidence. Only every other migrated trace is displayed. Frequencies 0–40 Hz were migrated and 13 traces where used in the absorbing boundary. The migration interval was 20 m.

$$P_1(\mathbf{r}, z, d, \omega) = \frac{1}{(2\pi)^2} \int_{-\infty}^{\infty} e^{-i\mathbf{k}_r \cdot \mathbf{r}} e^{ik_{z0} d} \tilde{P}_-(\mathbf{k}_r, z, \omega)\, d\mathbf{k}_r . \tag{29}$$

For $\Delta z = z_{n+1} - z_n$ sufficiently small, the integral of equation (28) can be evaluated using the trapezoid rule, which, after substituting $P_-(\mathbf{r}, z_{n+1}, \omega)$ for $P_1(\mathbf{r}, z_{n+1}, 0, \omega)$, results in

$$\int_{z_n}^{z_{n+1}} dz' \Delta u(\mathbf{r}, z')\, P_1(\mathbf{r}, z', z_{n+1} - z', \omega)$$

$$= \frac{\Delta z}{2} [\Delta u(\mathbf{r}, z_{n+1})\, P_-(\mathbf{r}, z_{n+1}, \omega)$$

$$+ \Delta u(\mathbf{r}, z_n)\, P_1(\mathbf{r}, z_n, \Delta z, \omega)]. \tag{30}$$

Substituting equation (30) into equation (28) gives

$$P_-(\mathbf{r}, z_{n+1}, \omega)\left[1 - \frac{1}{2} i\omega \Delta u(\mathbf{r}, z_{n+1})\Delta z\right]$$

$$= P_1(\mathbf{r}, z_n, \Delta z, \omega)\left[1 + \frac{1}{2} i\omega \Delta u(\mathbf{r}, z_n)\Delta z\right]. \tag{31}$$

Remembering that we have ignored terms on the order of $\Delta u^2(\mathbf{r}, z)$, equation (31) is equivalent to

$$P_-(\mathbf{r}, z_{n+1}, \omega) \exp [-(1/2)i\omega \Delta u(\mathbf{r}, z_{n+1})\Delta z]$$

$$= P_1(\mathbf{r}, z_n, \Delta z, \omega) \exp [(1/2)i\omega \Delta u(\mathbf{r}, z_n)\Delta z]. \tag{32}$$

Solving for $P_-(\mathbf{r}, z_{n+1}, \omega)$ gives

$$P_-(\mathbf{r}, z_{n+1}, \omega) = \exp \{(1/2)i\omega[\Delta u(\mathbf{r}, z_{n+1}) + \Delta u(\mathbf{r}, z_n)]\Delta z\} P_1(\mathbf{r}, z_n, \Delta z, \omega). \tag{33}$$

If we stop and consider the case where there is no vertical slowness variation in the depth interval Δz, i.e., $\Delta u(\mathbf{r}, z) = \Delta u(\mathbf{r})$ only, then

$$P_-(\mathbf{r}, z_{n+1}, \omega) = e^{i\omega \Delta u(\mathbf{r})\Delta z} P_1(\mathbf{r}, z_n, \Delta z, \omega), \tag{34}$$

where the spatial Fourier transform of $P_1(\mathbf{r}, z_n, \Delta z, u)$ is

$$\tilde{P}_1(\mathbf{k}_r, z_n, \Delta z, \omega) = \tilde{P}_-(\mathbf{k}_r, z_n, \omega)\, e^{ik_{z0}\Delta z}, \tag{35}$$

which are equations (9) through (12) used in the split-step migration described earlier.

EXAMPLES

We illustrate split-step Fourier migration with several examples. In all the synthetic data examples, the data were

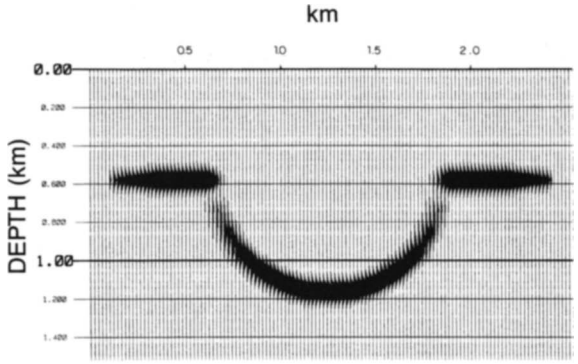

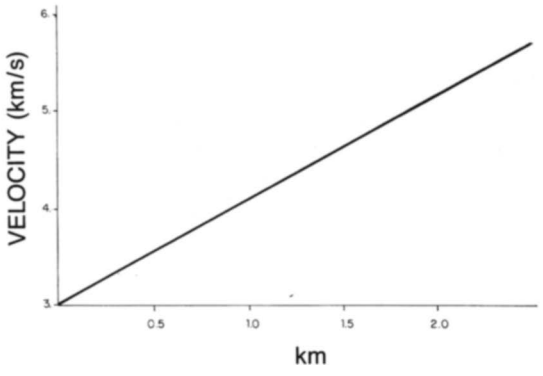

FIG. 2a. (upper) Exploding reflectors for a circular trough model used to generate the synthetic seismic data of Figures 2b, 3a, and 4. (lower) The laterally varying velocity function used to generate the synthetic data of (b).

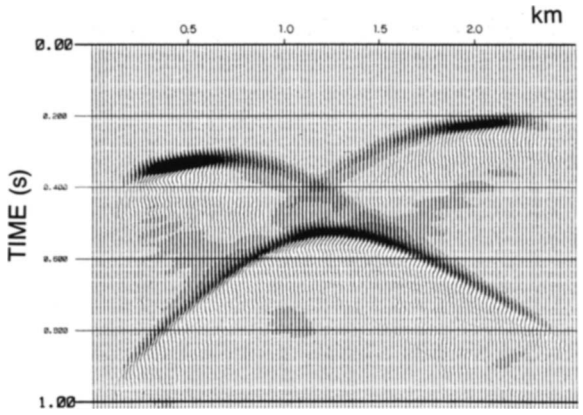

FIG. 2b. Synthetic data corresponding to the model of Figure 2a. 128 traces are shown with $\Delta x = 20$ m. The time sampling interval was 4 ms.

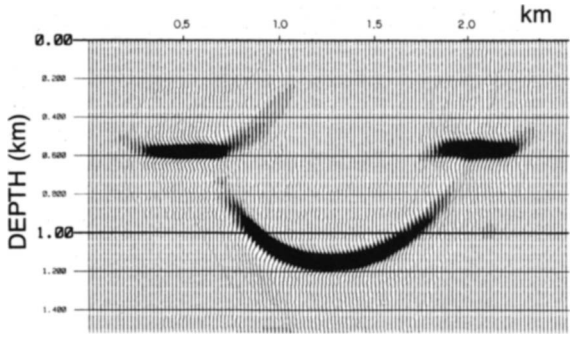

FIG. 2c. Data of (b) migrated using the split-step Fourier method. Frequencies 0–40 Hz were migrated and 13 traces were used in the absorbing boundary. The migration interval was 20 m.

generated using either ray-tracing or finite-difference modeling programs. All of the migration examples used the split-step migration method as defined by equations (34) and (35). To diminish reflections from the edge of the data, an exponentially damped taper was applied. This absorbing boundary condition was applied in the spatial domain for every frequency at every depth interval.

To test the ability of the method to accommodate lateral velocity changes, a 45-degree dipping reflector was used. Figure 1a (lower) shows the laterally varying velocity function used to generate the time section that was migrated, Figure 1a (upper). No vertical velocity variation is present. The model data were generated at a 4 ms time sample interval and with a trace separation of 20 m. Figure 1b shows every other trace of the migrated result. The solid line indicates the correct reflector position in depth. The deviation is greatest at the deepest point of the reflector, where the reflection events have a significantly nonvertical angle of incidence at the surface. In this example, the events are migrated with little error until the midpoint of the section. At the worst point, the deviation between the true and migrated dips is 1.5 degrees. The maximum lateral velocity variation in this example is 1.5 to 1, or a lateral slowness variation of 0.66 to 1. In this example we used 256 traces. Frequencies of 0 to 40 Hz were migrated and 13 traces were used in the absorbing boundaries. The migration interval was 20 m, and 113 depth samples were generated.

Figure 2a is an example of a semicircular trough where the velocity varies only laterally. Figure 2a (lower) shows the velocity function which varies linearly from 3.0 to 5.7 km/s, a velocity ratio of 1.9 to 1, i.e., a nonlinear lateral slowness perturbation of −31 to +31 percent. Figure 2a (upper) shows the initial exploding reflectors used by the finite-difference modeling program to generate the synthetic data of Figure 2b. Figure 2c is the migrated result using the split-step Fourier method. In this case the results are good, even though the total slowness perturbation is large, because the velocity varies slowly. In this example, frequencies from 0–40 Hz were migrated and 13 traces were used in the absorbing boundaries. The migration interval was 20 m, and 75 depth samples were generated.

To illustrate the effect of an abrupt velocity discontinuity, the same exploding reflector model was used but with the velocity function of Figure 3a (upper). The resulting finite-difference data are shown in Figure 3a (lower) and the migrated result is shown in Figure 3b. In this case, the velocity discontinuity is 10 percent and the slowness perturbation changes from −4.76 to +4.76 percent of the mean slowness. Although the method should not be able to accommodate such a rapid transition zone, the result is still good because the magnitude of the perturbation is small. If we increase the velocity discontinuity from 3 to 5.1 km/s, i.e., a slowness perturbation of 52 percent, the method fails (Figure 4) because of the magnitude and abruptness of the transition, even though the slowness perturbation is smaller in magnitude than the total slowness variations for the case of Figure 2. Note, however, that the horizontal events in Figure 4 are correctly positioned. Correct positioning would not be pos-

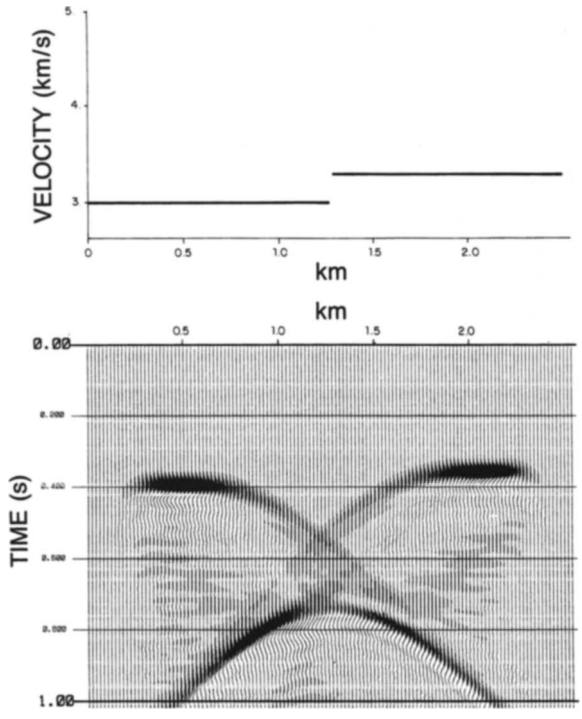

FIG. 3a. (upper) velocity model with a lateral discontinuity where the velocity changes from 3.0 km/s to 3.3 km/s. (lower) synthetic data corresponding to the exploding reflector model with this discontinuous velocity function. Data parameters are the same as Figure 2.

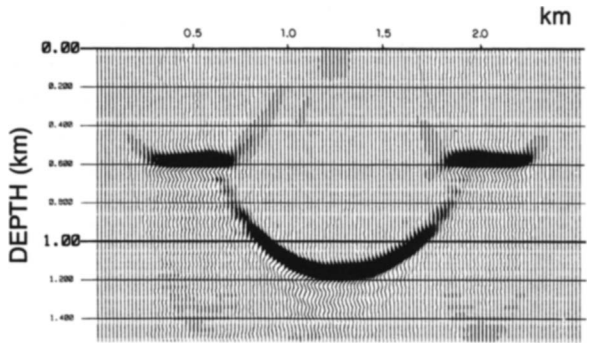

FIG. 3b. Data of (a) migrated using the split-step Fourier method. Reasonably good results are obtained because the velocity discontinuity is only 10 percent. Migration parameters are identical to those used in Figure 2.

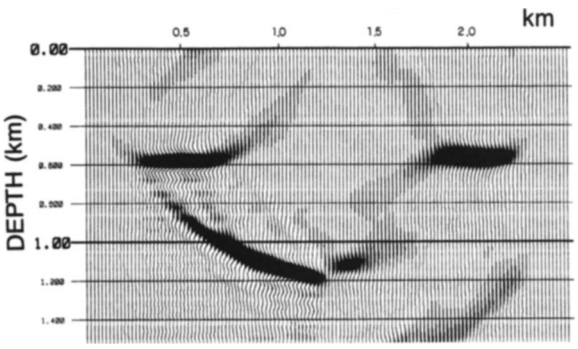

FIG. 4. Migration results for data similar to that of Figure 3, but for the case where the velocity changes discontinuously from 3 to 5.1 km/s. In this case the large and abrupt change is not taken into account properly by the split-step Fourier method. Data and migration parameters are the same as those used in Figures 2 and 3.

sible with ordinary phase-shift migration. In both examples, the data and migration parameters were identical to those used in the example shown in Figure 2.

A more realistic situation is illustrated by a finite-difference model of a salt dome. Figure 5a shows the model and the velocity function. The reflection coefficients were calculated from the vertical change in velocity. Figure 5b shows 256 traces of synthetic finite-difference data for a near-offset gather (source-receiver offset of 287.5 m). (For our purposes in this example, we have assumed that this is equivalent to a zero-offset section.) For these data, the trace separation is 25 m and the time sample interval is 2 ms. Figure 6 is the result of the split-step migration. The results are good even though there are considerable and abrupt lateral velocity variations in the vicinity of the salt dome,

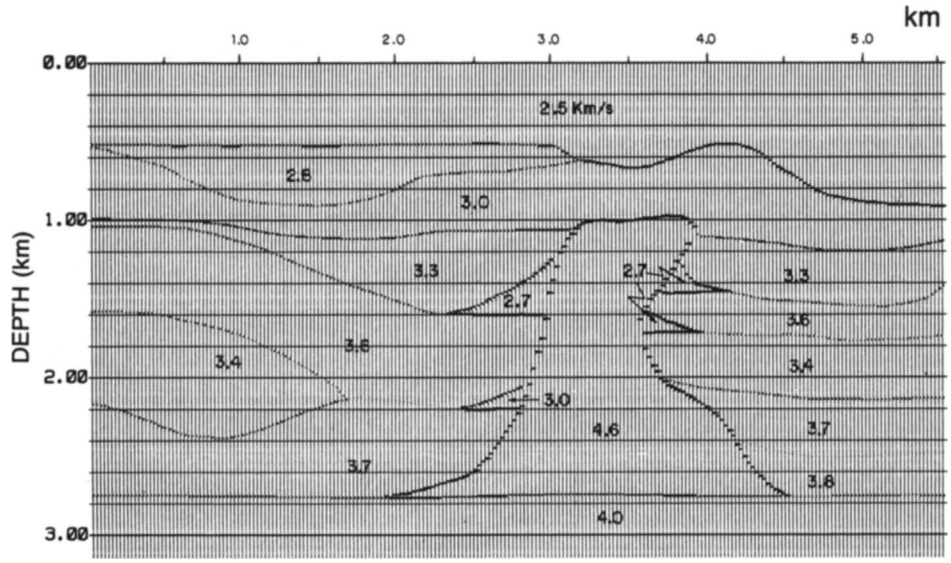

FIG. 5a. Interval velocities and reflector locations for a salt dome model. The reflector locations can be used to evaluate the migration results.

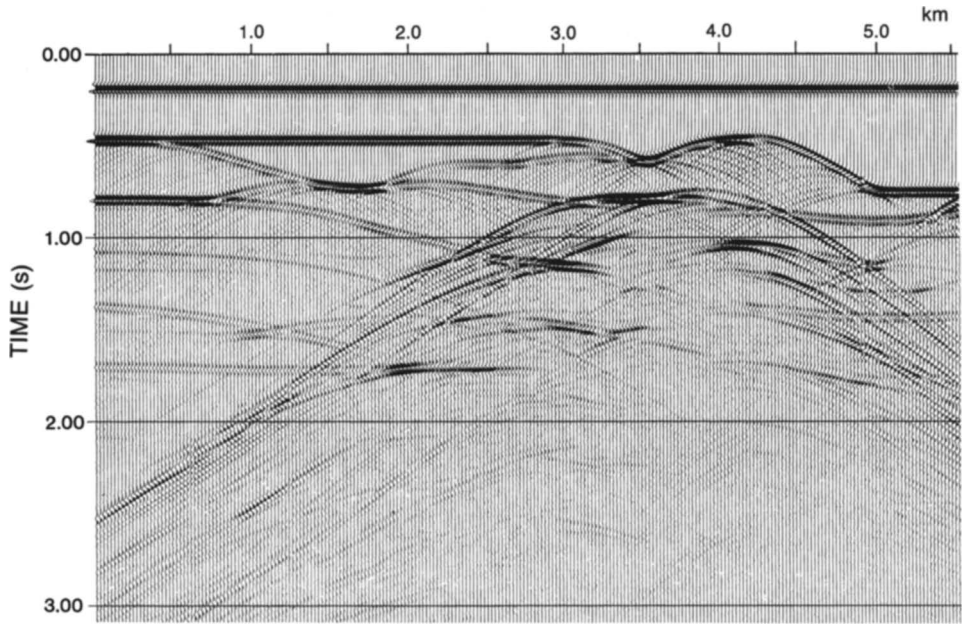

FIG. 5b. Synthetic finite-difference seismic data corresponding to the velocity model of (a). (Data provided courtesy of Mobil Research and Development Company.)

e.g., 2.7 to 4.6. In this example, frequencies of 0–40 Hz were migrated and eight traces were used in the absorbing boundaries. The migration interval was 5 m.

Figure 7 is a detailed comparison of the split-step method (left) with phase-shift migration for a laterally invariant velocity function (right). The reflectors of Figure 5a are superimposed on both plots for comparison. The split-step method has imaged the flanks of the salt dome successfully.

The French (1974) model was used to test the split-step method for 3-D migration. The data were generated using the Sierra Quick™ ray-trace modeling software to synthesize a zero-offset seismic section for the 3-D model. The trace and line spacing are 12.2 m, and the time sampling interval is 5 ms. 64 lines were generated with 128 traces per line. The model results are ray theoretical and do not include true diffraction effects. Figure 8 shows seismic line 9 before

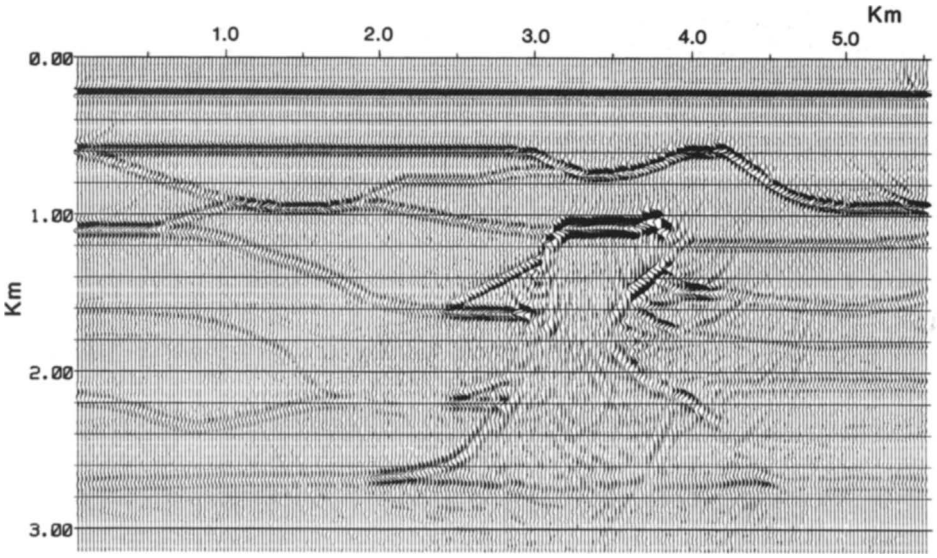

FIG. 6. Split-step migration of the data of Figure 5b. The result should be compared to the reflector locations in Figure 5a. Although some noise is present, the overall quality of the image is good even though the velocity constrasts are as high as 1.7 on the flanks of the dome. No smoothing of the velocity function was performed. Also, no time or trace interpolation was done. In this example, the input data consisted of 4 s of data sampled at 2 ms. The separation between traces was 25 m. The migration interval was 5 m. Frequencies 0–40 Hz were migrated. Only eight traces were used in the absorbing boundaries.

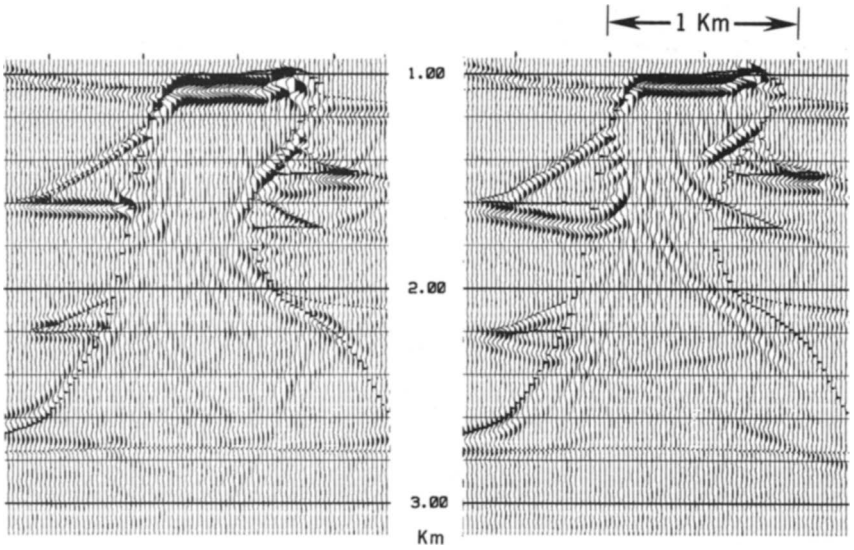

FIG. 7. Detailed comparison of the split-step migration (left) and a depth-only variable velocity phase-shift migration (right). The reflectors of Figure 5a are superimposed on both plots for comparison. Note the ability of the split-step method to image the flanks of the salt dome accurately.

(upper) and after (lower) the split-step Fourier 3-D migration.

In this example, frequencies 0–40 Hz were migrated and eight traces and eight lines were used in the absorbing boundaries. The migration interval was 1.83 m. The split-step migration uses the entire 3-D volume simultaneously, so that both inline and crossline events are migrated correctly, in contrast to 2-D by 2-D methods, which may be poor approximations in complex geologic situations. Note in this figure that the deepest event at 1100 m (bold arrow) is nearly horizontal, indicating that the overlying lateral velocity variations have been taken into account correctly. Only minor distortions occur under the intersection of the dome and the horizontal event.

Figure 9 shows a depth slice from the migrated volume. The position of the depth slice is indicated on the migrated depth section of Figure 8. The upper plot displays the theoretical locations of the reflectors generated by taking first differences of the velocity function. The lower plot is the split-step Fourier migration result. The spatial position of the final image is quite good.

Figure 10 is a real data example of 2-D split-step migration for data acquired in the Carolina Trough offshore the East Coast of the United States. Figure 10a shows the original stacked data in the vicinity of the continental shelf edge. The data were migrated to depth using the split-step method (Figure 10b) and then converted back to time by resampling to a 4 ms sample interval for comparison (Figure 10c). [For this migration example interval velocities were initially derived by interpreting the stacking velocities and using Dix's (1955) formula. The resulting interval velocities were then refined by transforming the CDP gathers to the τ-p domain and iteratively performing a τ-p NMO correction (Stoffa et al., 1981). The final interpreted interval velocities were then smoothed prior to migration.] In this example, 2048 traces separated by 12.5 m were migrated. The number of input time samples was 2048, and frequencies of 5 to 50 Hz were migrated. The migration interval was 16 m, and output depth samples were generated by interpolation every 8 m. Absorbing boundaries of 50 traces were used. Migration through the water column was done in one 800 m interval using a velocity of 1.5 km/s. The CPU time on a Cray X-MP/24 supercomputer was 1159 s to migrate to a depth of 8 km.

Figure 11 illustrates both 2-D and 3-D split-step migrations of 3-D data collected offshore Costa Rica. The diffractions are from the top of the accretionary prism complex (arrows) in this subduction zone. The upper section is part of a stacked line from the 3-D survey consisting of 512 traces, each separated by 33.3 m. These data were migrated to a depth of 6.9 km using the split-step algorithm and then converted back to time for comparison (middle). Although many of the diffractions from the rough surface of the accretionary prism complex have been removed, the image of the top of the prism complex is still distorted. Figure 11

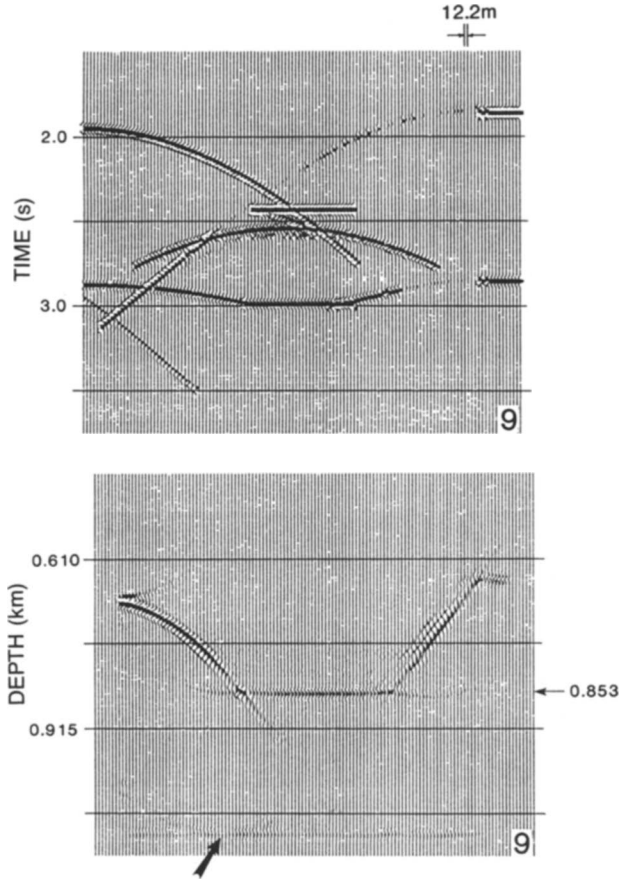

FIG. 8. (upper) Line 9 from the synthetic 3-D zero-offset data volume for the French (1974) 3-D model generated using the Sierra Quick™ ray-trace modeling software. (lower) 3-D split-step Fourier migrated result for Line 9.

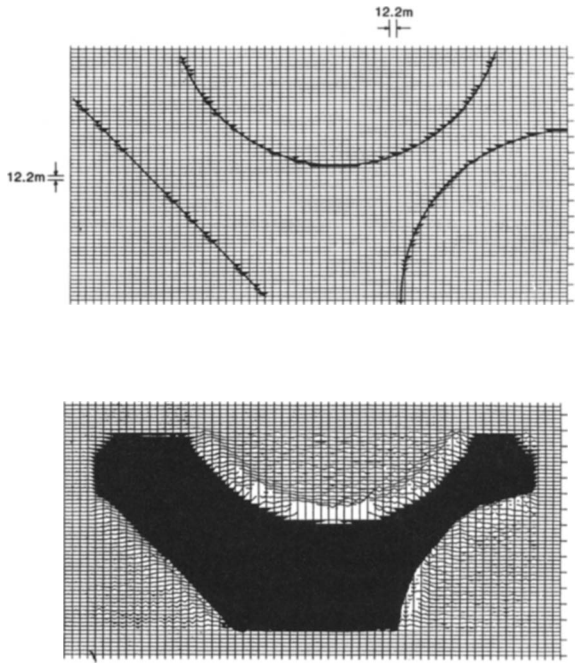

FIG. 9. (upper) Reflector locations for the French model obtained by taking first differences of the 3-D velocity field at a depth of 0.853 km. (lower) Corresponding depth slice after the split-step Fourier migration. The edges of each dome are correctly imaged. Figure 8 indicates the position of this depth slice in section format.

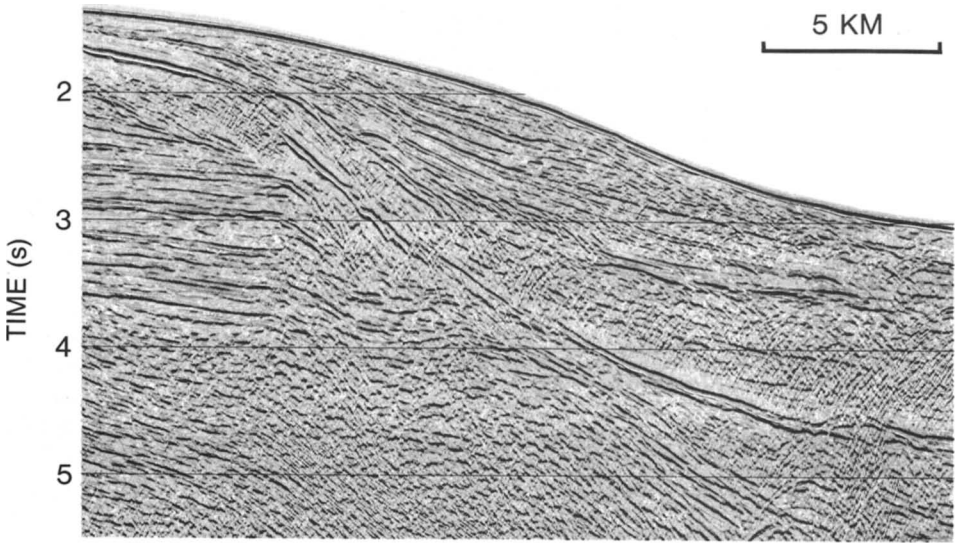

FIG. 10a. Stacked section collected over the continental shelf edge in the Carolina Trough region. 2048 traces with a separation of 12.5 m were used to migrate the data shown in (b). Only every other trace is displayed here (25 m display spacing).

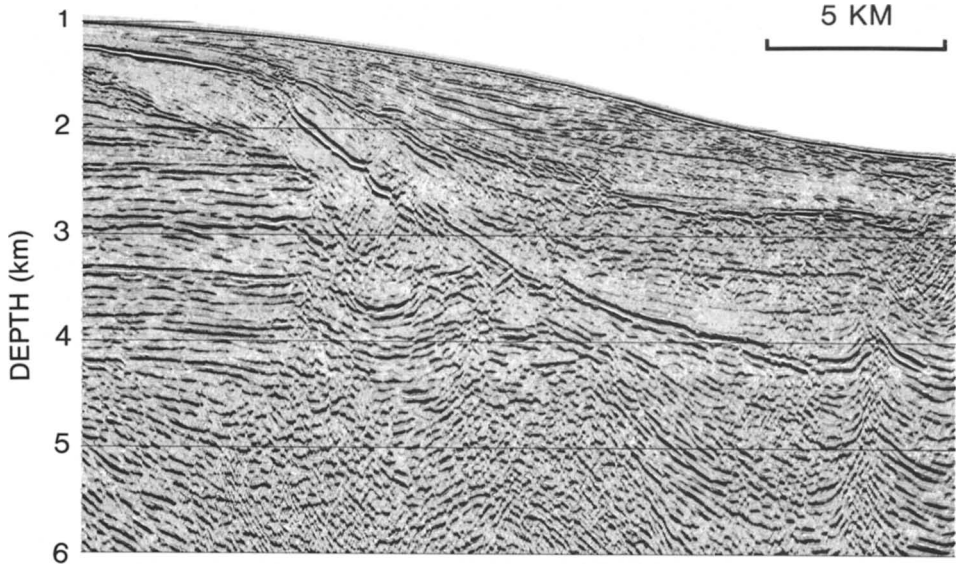

FIG. 10b. Depth migration of Carolina Trough data. Every other trace is displayed. Frequencies 5–50 Hz and absorbing boundaries of 50 traces were used in the migration.

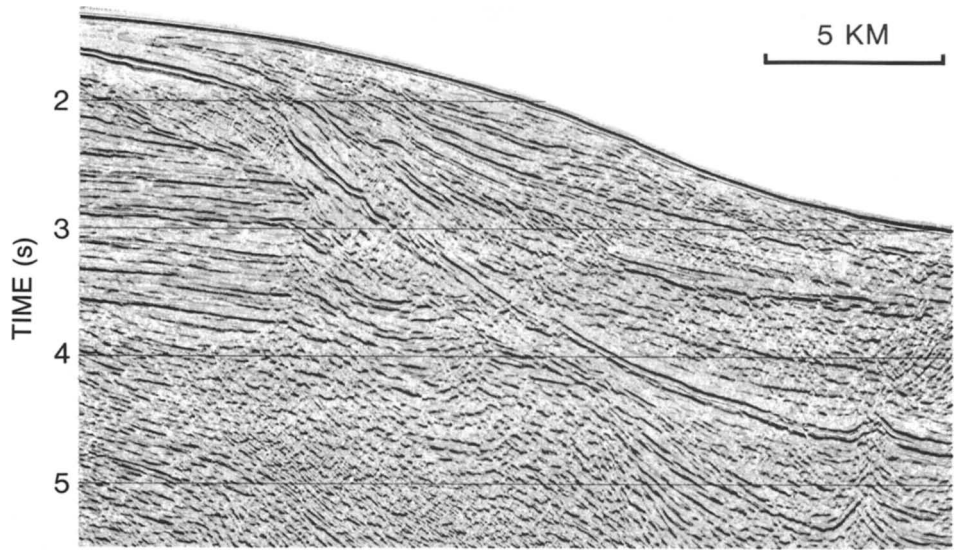

FIG. 10c. The depth-migrated Carolina Trough data of (b), converted to time by resampling. This time display allows a direct comparison with the original data of (a).

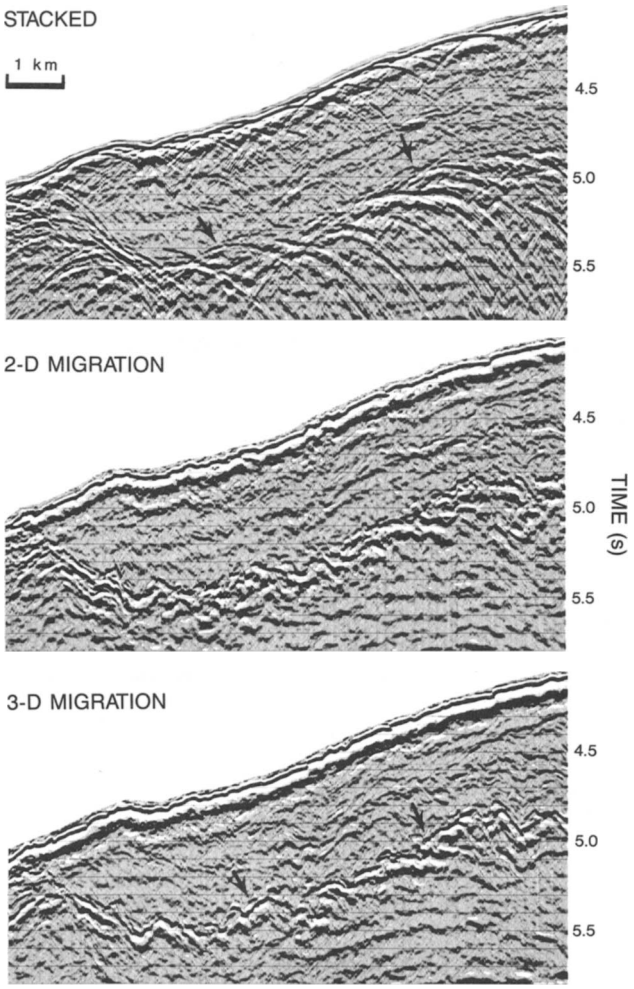

FIG. 11. Stacked 3-D data collected over the accretionary wedge offshore Costa Rica. 32 lines of 512 traces from the 3-D data volume were used to compare 2-D and 3-D split-step migrations. Each line has 512 traces with a spacing of 33 m. The line spacing was 50 m. (Upper) portion of stacked dip line in the middle of the 32 line data volume. (Middle) same line after 2-D split-step migration. The depth migrated data were resampled to time for comparison. (Lower) same line, after 3-D split-step migration of the 32 line data volume. Arrows indicate the top of the accretionary prism.

(lower) is a 3-D split-step depth migration of 32 lines each separated by 50 m. The data were then converted back to time for comparison. In the 3-D migration, the image of the top of the prism complex (arrows) has much better lateral continuity.

In both the 2-D and 3-D examples, migration through the water column was performed in one 2.5 km migration interval using a velocity of 1.5 km/s. The migration interval through the section was 80 m with output depth samples generated by interpolation every 8 m. The number of 4 ms interval input time samples was 2048, and frequencies of 5 to 45 Hz were migrated. The data were converted back to time by resampling to a 4 ms sampling interval. Absorbing boundaries of 45 traces and six lines were employed to minimize edge effects. The CPU time on a Cray X-MP/24 supercomputer was 82 s for the 2-D migration and 2915 s for the 3-D migration.

DISCUSSION

The split-step Fourier method offers an alternative to finite-difference migration methods. The method is similar to constant-velocity phase-shift migration but takes into account lateral velocity variations. Theoretically, the velocity must be slowly varying to be properly taken into account. Practical experience, however, indicates that data with even reasonably rapid velocity transitions can be imaged effectively. Unlike phase shift plus interpolation, which requires a constant-velocity migration for each velocity in the current depth extrapolation interval, the split-step Fourier method requires only one additional spatial Fourier transform. Like phase-shift migration, the method is unconditionally stable.

Some practical considerations can be used to improve the performance of the split-step migration method. First, only the frequencies that are well defined need to be migrated. Since the computation time and storage requirements are directly proportional to the number of frequencies used, limiting the frequencies to those that are well determined in the data reduces the computation time as well as the storage requirements.

Second, since we alternate between the frequency-wavenumber and frequency-space domains, various types of boundary conditions can be used to minimize edge effects. In all the examples shown, we simply applied an exponentially damped taper to the edge of the data volume in the space domain for each frequency during each downward continuation. Practical experience indicates that a taper length of one-eighth the number of traces per line gives reasonable results. More sophisticated boundary conditions, however, can also be implemented (Clayton and Engquist, 1980).

Third, it may be possible to move down to the zone of interest in one or several large steps using the mean slowness for each depth interval. For marine data this makes it possible to migrate through the water column in one step.

Finally, we note that since the computation is performed independently for each frequency, the migration of each frequency can proceed in parallel, and the results can be summed at the end of the computation for each depth. This makes it possible to consider implementations of the algorithm in parallel computer architectures.

ACKNOWLEDGMENTS

This work was partially developed as a research project in the PPPG program at Federal University of Bahia, Brazil. The support of Petrobras and the Brazilian agencies CNPA and Finep is acknowledged. A grant from Cray Research, Inc. supported the final part of the research and the National Science Foundation (NSF) grants OCE-8511364 and OCE-8711300 provided the support for the real data examples.

The University of Texas at Austin, Institute for Geophysics contribution number 801.

REFERENCES

Baysal, E., Kosloff, D. D., and Sherwood, J. W. C., 1983, Reverse time migration: Geophysics, **48**, 1514–1524.

Clayton, R. W., and Engquist, B., 1980, Absorbing boundary conditions for wave-equation migration: Geophysics, **45**, 895–904.

Dix, C. H., 1955, Seismic velocities from surface measurements: Geophysics, **20**, 68–86.
Freire, R. M. L., 1988, Migração Por Mudança de Fase em Duas Etapas, Ph.D. thesis, PPPG/UFBa, Salvador, Bahia, Brazil (in Portuguese).
French, W. S., 1974, Two-dimensional and three-dimensional migration of model-experiment reflection profiles: Geophysics, **39**, 265–277.
Gazdag, J., 1978, Wave equation migration with the phase-shift method: Geophysics, **43**, 1342–1351.
Gazdag, J., and Sguazzero, P., 1984, Migration of seismic data by phase-shift plus interpolation: Geophysics, **49**, 124–131.
Hardin, R. H., and Tappert, F. D., 1973, Applications of the split-step Fourier method to the numerical solution of nonlinear and variable coefficient wave equation: SIAM Rev., **15**.
Kosloff, D., and Kessler, D., 1987, Accurate depth migration by a generalized phase-shift method: Geophysics, **52**, 1074–1084.
Loewenthal, D., Lu, L., Robertson, R., and Sherwood, J., 1976, The wave equation applied to migration: Geophys. Prosp., **24**, 380–399.
McDaniel, S. T., 1975, Parabolic approximations for underwater sound propagation: J. Acoust. Soc. Am., **58**, 1178–1185.
Pai, D. M., 1985, A new solution method for wave equations in inhomogeneous media: Geophysics, **50**, 1541–1547.
——— 1988, Generalized *f-k* (frequency-wavenumber) migration in arbitrarily varying media: Geophysics, **53**, 1547–1555.
Stoffa, P. L., Buhl, P., Diebold, J. B., and Wenzel, F., 1981, Direct mapping of Seismic data to the domain of intercept time and ray parameter—A plane-wave decomposition: Geophysics, **46**, 255–267.
Stolt, R. H., 1978, Migration by Fourier transform: Geophysics, **43**, 23–48.
Tappert, F. D., 1974, Parabolic equation method in underwater acoustics: J. Acoust. Soc. Am., **55**, Supplement 34 (A).
Wen, J., McMechan, G. A., and Booth, M. W., 1988, Three-dimensional modeling and migration of seismic data using Fourier transforms: Geophysics, **53**, 1194–1201.

APPENDIX

ERROR CONSIDERATION FOR THE SPLIT-STEP FOURIER METHOD

The error in the split-step Fourier method can be analyzed based on the way the lateral slowness variations are decomposed into a reference slowness $u_0(z)$ and a perturbation $\Delta u(\mathbf{r}, z)$ and the way this perturbation is taken into account. First, the split-step Fourier method assumes that the perturbation term is sufficiently small with respect to the reference slowness for the current depth extrapolation interval Δz, so that terms on the order of $\Delta u^2(\mathbf{r}, z)$ can be ignored. For depth extrapolation across intervals where no slowness variation exists, i.e., $\Delta u(\mathbf{r}, z) = 0$, the method is exact and reduces naturally to the phase-shift migration method. When the slowness does vary in the depth interval, the principal error in the method can be attributed to the neglect of the second-order variations in the slowness and the higher order terms of equation (20) which are neglected in equation (21). Comparing equations (20) and (21), we find that this error ε is

$$\varepsilon = i\omega \int_{z_n}^{z_{n+1}} dz' \int_{-\infty}^{\infty} d\mathbf{k}_r' \Delta\tilde{u}(\mathbf{k}_r - \mathbf{k}_r', z') \tilde{P}_-(\mathbf{k}_r', z', \omega) \times \left\{ e^{i\omega u_0[1-(k_r'/\omega u_0)^2]^{1/2}(z_{n+1}-z')} - \frac{\exp\{i\omega u_0[1-(k_r/\omega u_0)^2]^{1/2}(z_{n+1}-z')\}}{[1-(k_r/\omega u_0)^2]^{1/2}} \right\}. \quad \text{(A-1)}$$

To find the order of this approximation, we expand the two square root terms in each of the exponentials within the brackets, drop all terms greater than second order, and expand the denominator term. The result is

$$e^{i\omega u_0(z_{n+1}-z')}\{e^{-1/2\, i\omega u_0(k_r'/\omega u_0)^2(z_{n+1}-z')} - e^{-1/2\, i\omega u_0(k_r/\omega u_0)^2(z_{n+1}-z')}[1 + 1/2(k_r/\omega u_0)^2 + \cdots]\}. \quad \text{(A-2)}$$

The leading exponential does not depend on k_r' and can be removed from the integral over k_r' in equation (A-1). Expanding the remaining exponentials and dropping all but the second-order terms, we have

$$1 - 1/2\, i\omega u_0(k_r'/\omega u_0)^2(z_{n+1}-z') - [1 - 1/2\, i\omega u_0(k_r/\omega u_0)^2(z_{n+1}-z')][1 + 1/2(k_r/\omega u_0)^2]. \quad \text{(A-3)}$$

Neglecting terms of order k_r^4, expression (A-3) reduces to

$$-\frac{1}{2} i(k_r'^2 - k_r^2)\frac{(z_{n+1}-z')}{\omega u_0} - \frac{1}{2}(k_r/\omega u_0)^2. \quad \text{(A-4)}$$

This reduces the error expression of equation (A-1) to

$$\varepsilon = \int_{z_n}^{z_{n+1}} dz'\, e^{i\omega u_0(z_{n+1}-z')} \int_{-\infty}^{\infty} d\mathbf{k}_r'[(k_r'^2 - k_r^2)(z_{n+1}-z')/2u_0 - ik_r^2/2\omega u_0^2 + 0(k_r^4) + 0(k_r'^4)] \times \Delta\tilde{u}(\mathbf{k}_r - \mathbf{k}_r', z')\, \tilde{P}_-(\mathbf{k}_r', z', \omega), \quad \text{(A-5)}$$

which shows that the second and higher order derivatives of the slowness perturbation with respect to the horizontal coordinates will be neglected.